AIMS Environmental Science, 3(2): 185-198.
DOI: 10.3934/environsci.2016.2.185
Received 23 February 2016,
Accepted 27 March 2016,
Published 29 March 2016

http://www.aimspress.com/journal/environmental

Research article

Enhancing water flux of thin-film nanocomposite (TFN) membrane by incorporation of bimodal silica nanoparticles

Zhe Yang [1,3], Jun Yin [2] and Baolin Deng [1,2,*]

[1] Department of Chemical Engineering, University of Missouri, Columbia, MO 65211 USA
[2] Department of Civil & Environmental Engineering , University of Missouri, Columbia, MO 65211 USA
[3] Department of Civil Engineering, The University of Hong Kong, Pokfulam Road, Hong Kong

*** Correspondence:** Email: DengB@missouri.edu; Tel: +1-573-882-0075; Fax: +1-573-882-4784.

Highlights

- We synthesized two different silica nanoparticles containing different sizes of internal pores.
- We incorporated the different nanoparticles into thin film layer in reverse osmosis membrane.
- Surface roughness and hydrophilicity increased when the added amounts of nanoparticles increased.
- Increasing water permeability with constant NaCl rejection can be observed.

Abstract: Modern reverse osmosis (RO)/nanofiltration (NF) membranes are primarily made of thin-film composites (TFC) fabricated through interfacial polymerization of m-phenylene diamine (MPD) and trimesoyl chloride (TMC) on a polysulfone (PSF) supporting membrane. In this study, two types of bimodal silica nanoparticles (~80 nm) with different internal pore structures were synthesized and incorporated into the polyamide (PA) thin-film layer during interfacial polymerization at concentrations varying from 0 to 0.1 wt%. The as-prepared membranes were characterized by scanning electron microscopy (SEM), atomic force microscopy (AFM), and attenuated total reflection Fourier transform infrared (ATR FT-IR) spectroscopy, and their performances were evaluated in terms of the water permeability and salt rejection. The results showed the water permeability increased with increasing BSN concentrations, reaching a maximum of 53.5 L m^{-2} h^{-1} at a bimodal silica nanoparticle (BSN) concentration of 0.5 wt% (pressure at

300 psi, NaCl concentration: 2000 ppm). This represented a flux increase of approximately 40%, while a near constant salt rejection of 95% was maintained. The study demonstrated that the internal micro-mesoporous structures of bimodal silica nanoparticles contributed significantly to the membrane performance, which is consistent with previous studies with relatively uniform internal pores.

Keywords: Bimodal silica nanoparticles; interfacial polymerization; polyamide; water purification, thin-film nanocomposite

1. Introduction

Development of human society needs water, and desalination is one of the most effective ways to meet this ever increasing need [1,2]. In comparison with multi-stage flash (MSF), multiple effect distillation (MED) and hybrid (MSF/MED-RO) [3], reverse osmosis (RO) has dominated the recent global desalination market. An ideal thin-film composite (TFC) membrane should have high water flux and salt rejection, as well as good chlorine tolerance, anti-fouling resistance, and thermal stability [4-7]. TFC consists of a thin-film layer supported on a porous substrate (support layer). Polyamide (PA) thin-film is particularly effective to reject salt and organics and could be operated in a wide range of temperature (0 ℃–45 ℃) and pH (from 1 to 11) [8].

Much effort has been devoted to improve the performance of RO membrane by changing physicochemical properties of thin-film layer [9-17]. A common approach is to make the thin-film layer more hydrophilic, which may lead to an increased water flux and enhanced anti-fouling properties [9].

With the advent of nanotechnology, thin-film nanocomposite membrane (TFN) has recently attracted significant attention, as some nanoparticles embedded into the thin-film layer were found to enhance the membrane's mechanical property and sometime water flux and salt rejection [18,19]. By incorporating nanoparticles into the polyamide thin film layer of a RO or NF membrane, where diffusion controls the transport process, the goal is to essentially reach the percolation threshold in the dense rejection layer with an individual particle [17]. Jeong et al. [20] introduced Zeolite-A nanoparticles (NPs) into PA thin-film, leading to a high water flux with constant salt rejection. Other studies examined the impact of different diameters of sphere silica [21], TiO_2 NPs [22], multi-walled carbon nanotubes (MWNTs) [23], carbon nanotubes [24] and ordered mesoporous silica NPs [18,25-27]. It has been reported that both the hydrophilic property and the internal mesoporous structure of NPs played a significant role in the enhanced performance of TFN membranes [26,27].

In this study, we aimed at understanding if the incorporation of bimodal silica nanoparticles into thin-film layer would influence the membrane performances. Bimodal micro-mesoporous materials have large and small pores that could facilitate rapid fluid transport [28]. Here we first synthesized micro-mesoporous bimodal silica nanoparticles with a particle diameter of 40–90 nm. A series of TFN membranes were then developed *via* interfacial polymerization of m-phenylene diamine (MPD) and trimesoyl chloride (TMC), where BSNs were dispersed in TMC-hexane solution. The BSNs and TFN membranes were characterized by scanning electron microscopy (SEM), transmission electron

microscopy (TEM), atomic force microscopy (AFM), attenuated total reflection Fourier transform infrared (ATR FT-IR) spectroscopy, contact angle and N_2 absorption and desorption. The effect of micro-mesoporous structure was explored by evaluating the performance of TFN membranes embedded with two types of BSNs.

2. Materials and methods

2.1. Materials

Nonaethyleneglycol dodecylether ($C_{12}EO_{9,}$ 99%, Sigma-Aldrich), eicosaethyleneglycol octadecyl ether ($C_{18}EO_{20,}$ Sigma-Aldrich) and tetraethyl orthosilicate (TEOS, 98%, Sigma-Aldrich) were used as surfactants and silica source, respectively, for the synthesis of BSN-T. $C_{12}EO_{9,}$ polyoxyethylene (20) sorbitan monostearate (Tween 60, 99%, Sigma-Aldrich), and TEOS were used for the synthesis of BSN-C. Polysulfone (PSF) (Mw = 35,000, Aldrich) pellets dissolved in N,N-dimethylformamide (DMF, 99.8%, Aldrich) were used as the casting solution to make the support layer. MPD, (>99%, Aldrich) and TMC, (>98.5%, Aldrich) were the monomers used in the interfacial polymerization process. Sodium dodecyl sulphate (SDS, analytical grade, Sigma-Aldrich) was used as a NPs dispersion surfactant. Deionized (DI) water produced by a Millipore DI system (Synergy 185, 18.2 MΩ cm) was used for solution preparation and the filtration studies.

2.2. Preparation of BSN-T and BSN-C

BSNs were synthesized by a procedure reported in the literature [28]. A mixture of $C_{12}EO_9$, $Tween_{60}$, and H_2O at a molar ratio of 1:1:60 was mixed for 20 min at 60 °C, followed by the addition of TEOS. When the solution was cooled to 20 °C, the resulting pasty liquid-crystal (LC) was water-insolubilized by aging for 1 h at 20 °C. Then the transparent pre-aged LC phases were immersed in water at 1:250 TEOS, followed by addition of ammonium acetate at an 8:1 molar ratio of ammonium to $C_{12}EO_{9.}$ The aqueous pH was maintained at 6.6 by adding ammonium acetate. Additional water was added to extract the ethanol produced by the hydrolysis of TEOS and also to promote the condensation reaction. The final material immersed in water was maintained at 20 °C for 7 d. After that, the resulting fully aged soft gel was filtrated, washed initially with water and then repeatedly with ethanol before drying under vacuum. The BSN-T thus obtained were calcined at 400 °C for 30 min to remove the organic residuals. The reaction in the TEOS/$C_{12}EO_9$/$C_{18}EO_{20}$/H_2O system was carried out by a similar procedure using the TEOS/$C_{12}EO_9$ ratio of 4 and $C_{18}EO_{20}$ instead of Tween60. For a comparative study, $C_{12}EO_9$-free LC phases in both systems were also prepared. The final products (BSN-T and BSN-C) were stored in a desiccator.

2.3. Synthesis of PSF support layer and TFN membrane

The PSF support layer was prepared by the phase inversion method by using 15 wt% PSF-DMF casting solution. The casing solution was heated and stirred at 50 °C for 6 h, and kept overnight for degassing. The final solution was put on a glass plate and casted by casting knife (EQ-Se-KTQ-150, MTI Corp., Richmond, CA) to approximately 0.1 mm of film thickness. The glass plate with casing

solution was immediately immersed into a DI water bath (25 °C). The PSF support membrane was precipitated during phase inversion. Then, it was washed and kept in DI water for at least 24 h until use.

To fabricate TFN membranes, the stored PSF membrane was immersed in a 2.0 wt% MPD-water solution for 3 min. Extra solution on the surface was removed by a rubber roller. Then, the PSF support layer with MPD on the surface was placed in a 0.15 wt% TMC-Hexane solution sealed in lab bottle for 1min, followed by the formation of a PA thin-film layer. TMC-hexane solution containing NPs was treated by ultrasonication for 1 h before the IP process. Then, the obtained TFN membrane were rinsed with pure hexane and post-treated in an oven at 80 °C for 5 min, and then stored in DI water at 5 °C. The final products were named as BSN-T-TFN-x or BSN-C-TFN-x, where x indicated the concentration of NPs in TMC solution during the interfacial polymerization process.

2.4. Characterization and performance assessments

N2 adsorption and desorption from the two NPs were carried out on QUADRASORB^{TM} SI (Quantachrome Instruments, Boynton Beach, FL) at 77 K. The specific surface areas and pore size distributions were calculated by Brunauer–Emmett–Teller (BET) method and density functional theory (DFT) method, respectively. Internal structures of NPs were evaluated by TEM (JEOL 1400, JEOL Ltd., Peabody, MA). TEM samples of NPs were prepared by dropping NPs-ethanol mixture solution onto carbon coated copper grid and drying at room temperature. The size distribution of the particles and point of zero charge (PZC) were measured by dynamic light scattering (DLS) using a Zetasizer Nano measurement, where water was used as the disperse medium.

SEM analysis of the membrane surface was conducted using a piece of membrane dried at room temperature. The SEM specimen was prepared by placing the membrane (0.5 cm × 0.5 cm) onto a sample holder. After complete drying at room temperature, the specimen was coated with platinum by a sputter coater (K575x, Emitech Ltd., Kent, England) at 20 mA for 1 min to increase conductivity. The hydrophilicity of membrane surface was assessed based on the measurement of pure water contact angles by the sessile drop method using a video contact angle system (VCA-2500 XE, AST products, Billerica, MA). The contact angle was obtained as the average of at least five measurements at different locations on each membrane.

The functional groups of membrane surface were identified by attenuated total reflection Fourier transform infrared (ATR FT-IR) spectroscopy. Nicolet 4700 FT-IR (Thermo Electron Corporation, Waltham, MA) equipped with multi-reflection Smart Performers ATR accessory was used for this analysis. All spectra included the wave numbers from 500 to 4000 cm^{-1} with 128 scans at a resolution of 2 cm^{-1}. Quantitative surface roughness of the membrane was analyzed by atomic force microscopy (AFM5500, Agilent Technologies, Inc. Santa Clara, CA) with tapping mode in air. A 2 × 2 μm functional of surface area was tested and the root mean square (RMS) roughness was recorded.

A high pressure cross-flow filtration system (pressure range: 50–500 psi) was used to evaluate water flux and solute rejection.

The filter holder (Model: XX4504700, stainless steel, Millipore Corp., Billerica, MA) in the test

apparatus had an effective membrane area of 9.6 cm^2. Before data collection, each membrane was compressed by DI water at 300 psi until the water flux became stable. Water flux was calculated according to the weight change of permeate water with time at a constant transmembrane pressure (TMP). The weight of permeate water was measured by an Ohaus digital balance and recorded by a LabVIEW automated system (National Instruments LabVIEW 8.2). After the pure water flux test, salt solution (final concentration of 2000 ppm of NaCl) was added and the conductivity of feed and permeate solutions was measured by a conductivity/TDS meter (HACH Company, Loveland, CO). The measurement was conducted at 25 ± 1 °C, which was controlled by a water circulator (Isotemp 6200 R20F, Fisher Scientific, Inc., Pittsburgh, PA). The flux and rejection was calculated with Equation (1) and Equation (2), respectively.

$$\mathrm{J} = \frac{V_p}{A \times t} \tag{1}$$

$$\mathrm{R} = \left(1 - \frac{C_p}{C_f}\right) \times 100\% \tag{2}$$

where J is the permeability (L m^{-2} h^{-1}), V_p the permeate volume (L), A the membrane area (m^2) t the testing time (h). R the rejection percentage, and C_p and C_f the conductivities of permeate and original solution, respectively.

3. Results and discussion

3.1. Characterization of NPs

TEM (Figure 1) images of both BSN-T and BSN-C indicated that the silica nanoparticles had a near spherical shape. The size of each individual particle was around 40–90 nm with irregularly arranged micropores and mesopores, consistent with what was reported in the literature [28].

Figure 2 shows the N2 adsorption/desorption isotherm and pore size distribution of BSN-T and BSN-C. The specific surface area measured by the BET method was 435 m^2/g for BSN-T, 1208 m^2/g for BSN-C, indicating a significant difference in the internal structures between the two NPs. There were micropores for both NPs with a diameter around 1.8 nm. However, BSN-T had mesopores of around 2.5 nm, whereas BSN-C had larger mesopores, around 4 nm. The morphological observations were consistent with the pore distribution obtained from BET data. The result of DLS measurement suggested that BSN-T and BSN-C had mean diameter of 168 and 184 nm, respectively, which was significantly larger than the diameters observed from TEM. This difference could be caused by the hydration layer of water on the particle surface and potential aggregation of BSNs during the DLS measurement [27]. The DLS measurement also indicated that the point of zero charge (PZC) on the surface of these BSNs was 2.23, in agreement with the NPs being-silica in nature [29].

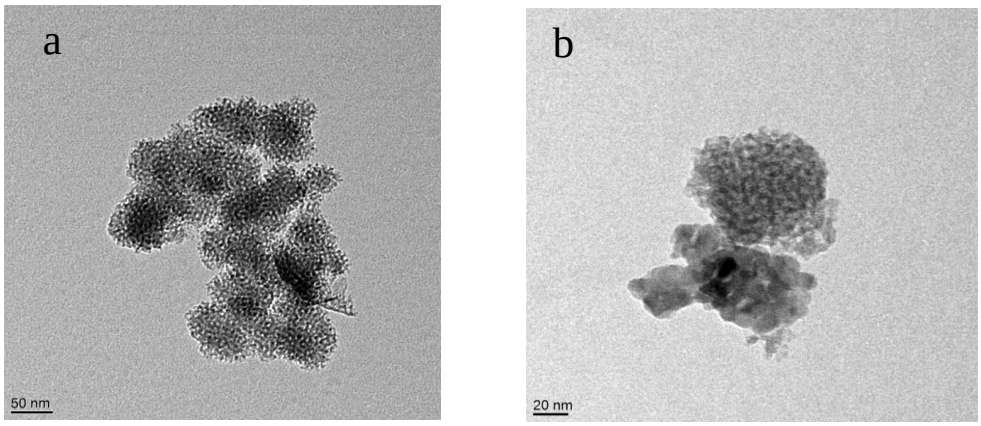

Figure 1. TEM images of NPs: (a) BSN-T; and (b) BSN-C.

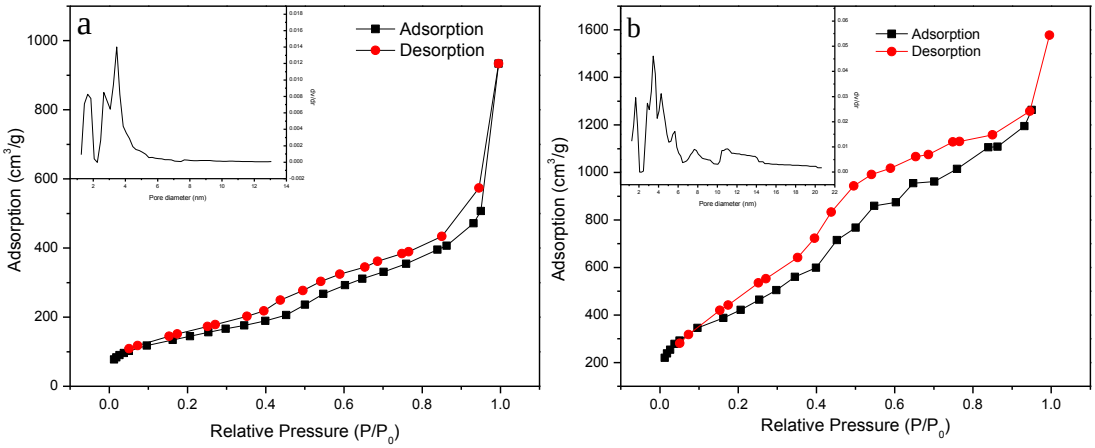

Figure 2. N_2 adsorption/desorption isotherm and pore size distribution of: (a) BSN-T; (b) BSN-C.

3.2. Characterization of TFN membranes

The ATR FT-IR spectra of the PSF support layer, TFC and BSN-S-TFN-0.05 (at loading concentration of 0.05 wt%) membranes are presented in Figure 3. For the PA thin-film layer on top of PSF support layer, peaks at 1660 cm^{-1} could be assigned to amide I C=O stretching vibration of amide, 1547 cm^{-1} to amide II, in-plane N-H bending and C-N stretching vibrations, 1610 cm^{-1} to N-H stretching of amide and 1450 cm^{-1} to C=O stretching and O-H bending of carboxylic acid [12,30,31]. Peaks between 1040 and 1080 cm^{-1}, derived from the asymmetric vibration of Si-O-Si [21], showed up in 0.05 wt% BSN-T and BSN-C. Additionally, a small peak appeared around 950 cm^{-1} in the 0.05 wt% BSN-T and BSN-C, which could be explained by the stretching vibration of Si-OH [32]. These results confirmed the presence of BSNs on the surface of the membrane. There was no other peak shown on the ATR FT-IR spectra suggesting that the absence of

strong chemical bonding between the NPs and polymer functional groups.

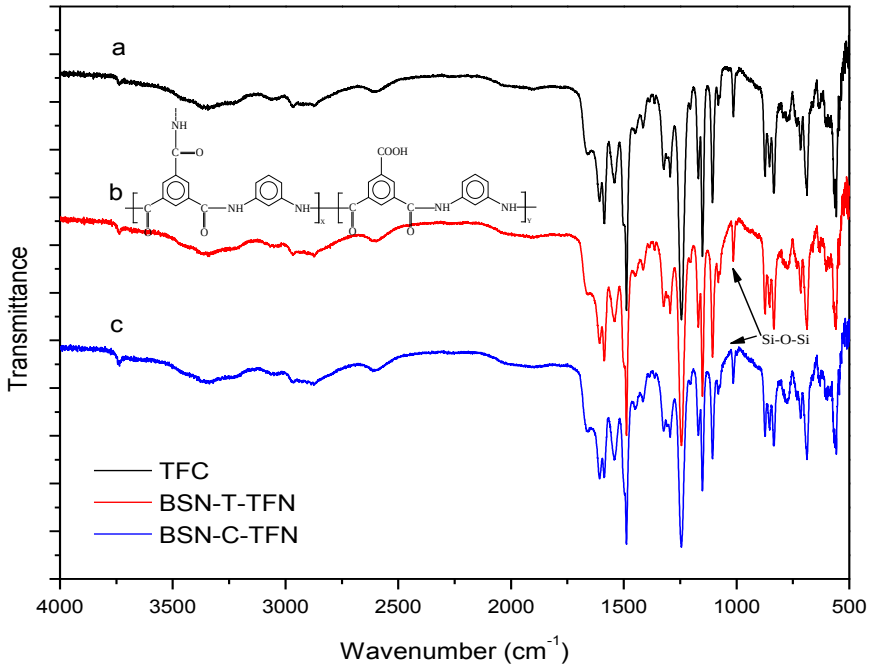

Figure 3. ATR FT-IR spectra of: (a) TFC; (b) BSN-T; (c) BSN-C.

Representative SEM images of the PSF support layer, TFC and TFN membranes with different concentrations of BSNs are shown in Figure 4. TFN membranes showed higher surface roughness than that of TFC membrane. The increased roughness could be the result of NP agglomeration on the membrane surface. In Figure 4a, pores with diameter around 20 nm were clearly visible on the PSF support layer surface. After the IP process, a PA thin-film layer generated by reaction between MPD and TMC covered the PSF surface, resulting in a leaf-like morphology (Figure 4b–h). With increasing BSNs concentration, severe agglomeration could occur (Figure 4c–e). The agglomeration of BSNs at a concentration of 0.05 wt% was not obvious (Figure 4d), especially when compared to the case with 0.1% BSNs (Figure 4e). In other words, BSNs agglomeration became a significant problem in the system with 0.1% or higher BSNs. A lower concentration of BSNs results in a better dispersion of BSNs in the thin-film layer.

Figure 5 shows the water contact angles of the TFN membranes with various amounts of BSNs. With increasing BSNs concentration, the contact angle of the membrane surface decreased first, reaching a minimum around 0.05 wt%, then leveling off (BSN-C-TFN) or rising up again (BSN-T-TFN). It appeared that the BSNs aggregation results in a decrease in the TFN membrane hydrophilicity. When the concentration of BSNs was further increased (>0.5 wt%), the aggregate formation of BSNs became so significant in the TMC-hexane solution that no functional membranes could be formed under the testing condition.

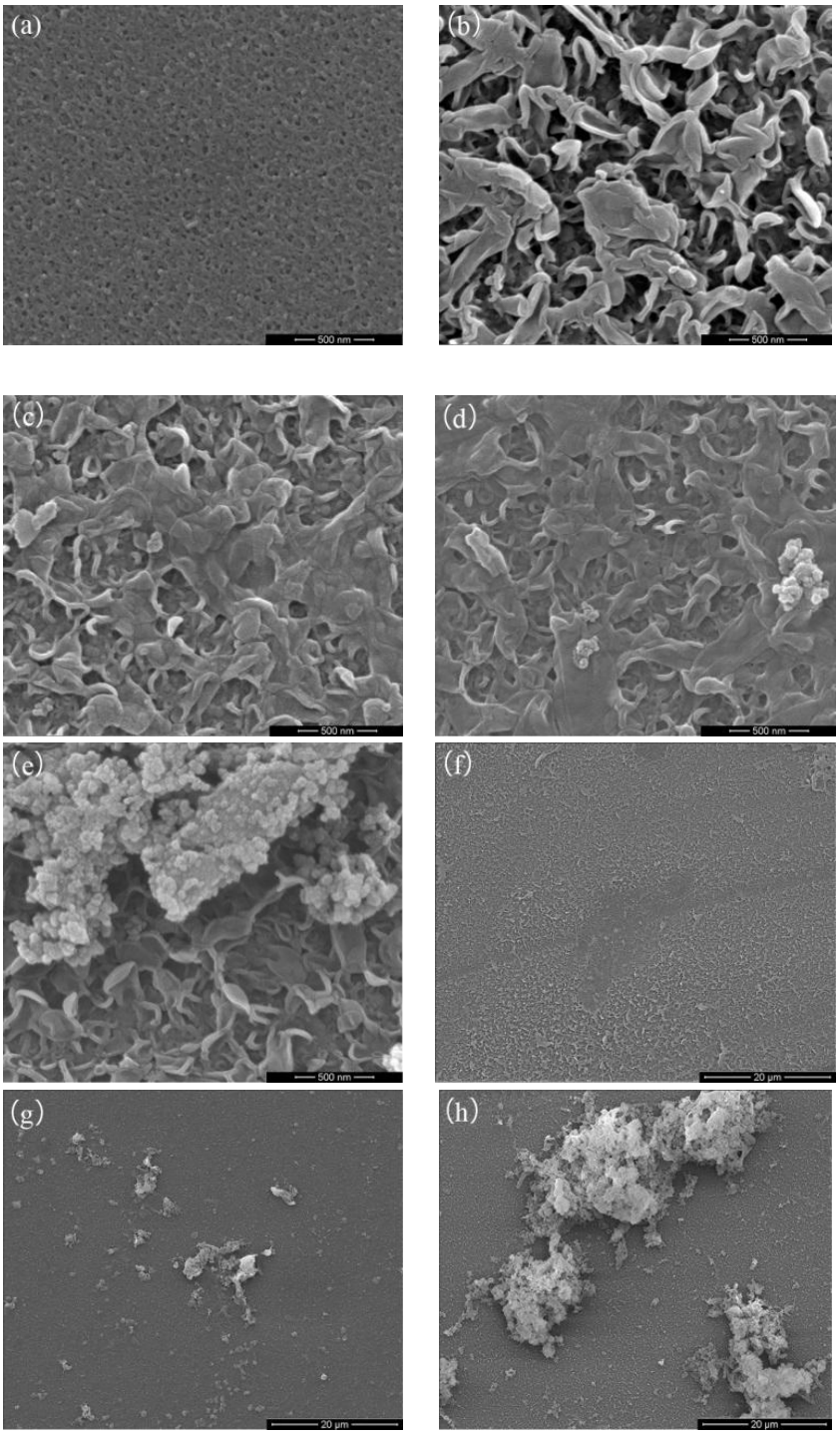

Figure 4. SEM images of BSN-T-TFN membranes: (a) PSF (500 nm); (b) TFC (500 nm); (c) BSN-T-0.01 wt% (500 nm); (d) BSN-T-0.05 wt% (500 nm); (e) BSN-T-0.1 wt% (500 nm); (f) TFC (2 μm); (g) BSN-T-0.05 wt% (2 μm); (h) BSN-T-0.1 wt% (2 μm).

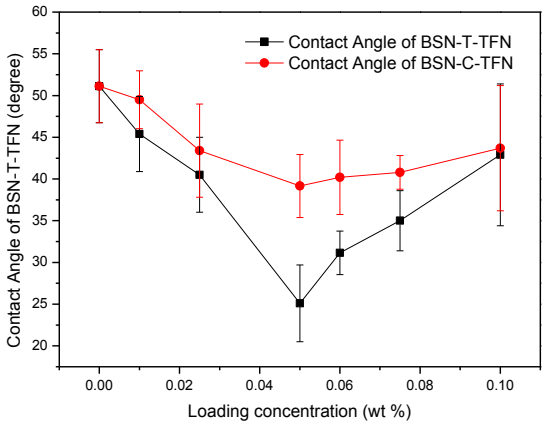

Figure 5. Contact angles of the TFN membranes as a function of of BSNs loading.

An AFM study was also conducted in this work to evaluate the topography of membrane samples (Figure 6). The PSF support layer showed a much smoother surface than that of TFC and TFN membranes. The measured RMS roughness was around 8.64 nm for the PSF support layer, 25.4 nm for the TFC and 43.1 nm for the TFN membrane, indicating that PSF support layer had a much smoother surface. The higher roughness of the TFC was caused by the leaf-like morphology of the PA thin-film layer and the presence of BSNs is believed to further increase the roughness.

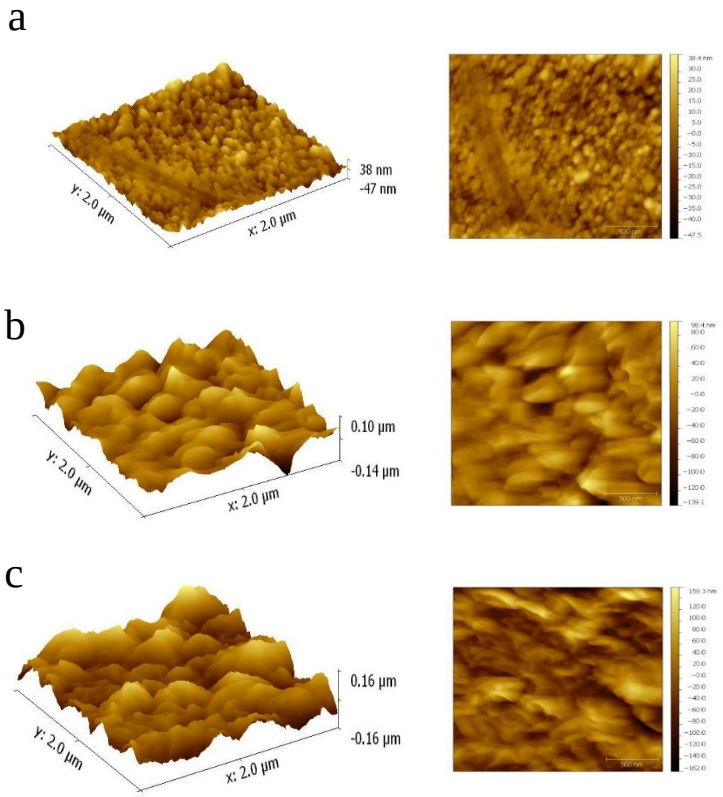

Figure 6. AFM images of the surfaces of membranes: (a) PSF; (b) TFC; (c) BSN-T-0.05 wt%.

3.3. Membrane water permeability and salt rejection

To understand the influence of the BSNs concentration on membrane performance, TFN membranes were fabricated in the system with increasing amounts of BSNs in the TMC hexane solution (0.01, 0.025, 0.05, 0.06, 0.075, 0.1 wt%). The membrane performance was assessed in terms of water permeability and NaCl rejection. The tests were conducted with 2000 mg/L NaCl solution under 300 psi (20.4 atm) of trans-membrane pressure (TMP). As shown in Figure 7b, with increasing BSN-C concentration, the water flux of the membranes increased from an initial value of 38 ± 2.2 L m^{-2} h^{-1} (without BSNs) to a maximum of 53.5 ± 5.5 L m^{-2} h^{-1}, and then decreased to 42.5 ± 3.5 L m^{-2} h^{-1} with a further concentration increase to 0.1 wt%. Membranes with BSN-T demonstrated a similar behavior (Figure 7b), showing a water flux of 49 ± 2.3 L m^{-2} h^{-1} at 0.05 wt% but decreased with a further increase in BSN-T loading. It was interesting to note that under all loading concentrations of both BSN-C and BSN-T, the rejection of NaCl remained almost constant at around 95 ± 1.2%.

The observed improvement of water flux in the presence of appropriate amounts of BSNs correlated to the membrane contact angle (Figure 5). The increased water flux as the loading concentration of BSNs increases from 0.01 to 0.05 wt% may be caused by the hydrophilic groups on the surface of the BSNs which improve the hydrophilicity of the membrane surface. This improved hydrophilicity facilitated the solubilization and diffusion of water molecules into the membranes. The incorporated BSNs may also deteriorate the formation of the densely-crosslinked PA thin-film structure, resulting in an increase of water flux. Additionally, BSNs in PA thin layer would cause defects around the nanoparticles and non-homogeneous thin layer thickness. Based on the results in Figure 6, the increased RMS roughness indicates larger surface area, and the water molecules could transport through a larger area. However, when the amount of BSNs in the TMC-hexane solution was increased over 0.05 wt%, the water flux of both TFN membranes decreased significantly. The TFN membrane with greater than 0.05 wt% BSNs loading concentration had visible agglomeration of the NPs on the surface of the TFN membrane. The aggregation of BSNs could reduce accessible surface area of the membranes compared to that of uniformly dispersed BSNs. Consequently, loading concentration of BSNs above 0.05 wt% lead to a decrease in both water permeability.

To address the aggregation problems seen with the NPs in TMC-hexane solution when the mass concentration of NPs is over 0.05 wt%, 1 mg/mL of sodium dodecyl sulphate (SDS) was added into TMC-hexane solution. It has been reported that SDS surfactant can mitigate the aggregation problem [33]. The results suggest the surfactant plays a distinctive role in the TFN membrane properties. Membranes prepared with surfactant SDS exhibited higher water permeability (from pristine 40 ± 2.83 to 41.85 ± 1.13 L m^{-2} h^{-1}) but lower salt rejection (from pristine 94.8 ± 1.14 to 91.29 ± 0.89 %). These results are attributed to the non-uniform distribution, severe aggregation and precipitation of BSNs in the TMC-hexane solution without SDS surfactant. The uniform dispersion of the BSNs with SDS at higher concentration results in a higher surface area of BSNs, thus the permeability increases. However, the selectivity deteriorated, which was caused by the damage to the structure of PA by the BSNs.

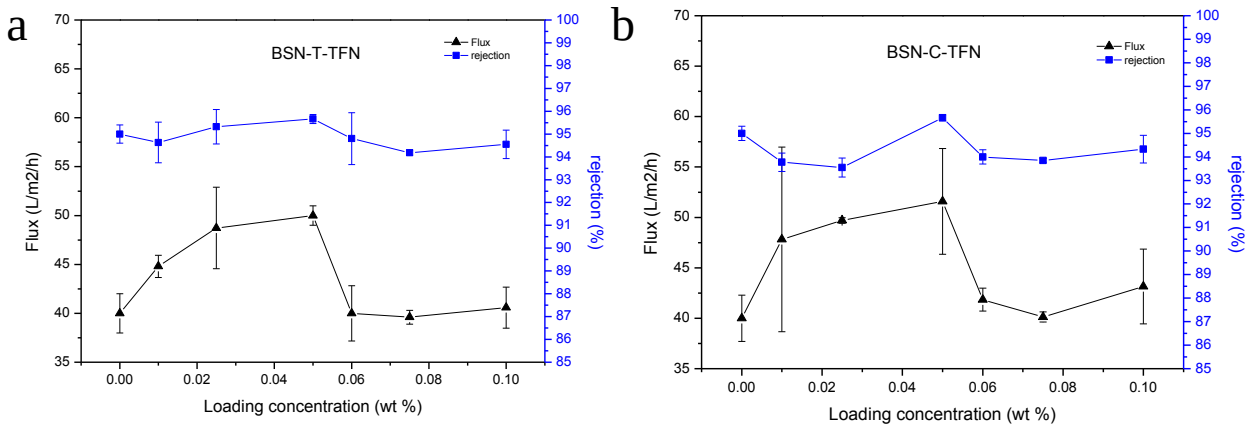

Figure 7. Water permeability and salt rejection: (a) BSN-T; (b) BSN-C.

It is meaningful to compare the performance of membrane prepared in this study with those reported in the literature (Table 1). The membrane with bimodal silica was found to have a water flux and salt rejection comparable to those with MCM-41 silica and graphene oxide (GO), and better than those with carbon nanotubes. As summarized in a recently review [34], a number of mechanisms might have contributed to the observed performance enhancements by incorporating nanoparticles into the membranes: 1) increased surface hydrophilicity leading to better water solubilization and diffusion, 2) reduced cross-linking intensity of active layer, and 3) additional water paths provided by the internal pores of nanofillers. Our original hypotheses were that the bimodal silica nanoparticles could increase membrane surface hydrophilicity and provide both micropores and mesopores as additional water paths for water flux enhancements. What we observed that the effect of BSNs are quite comparable to MCM-41 NPs with mesopores only, suggesting that the micropores within the bimodal silica nanoparticles might be too small to contribute significantly to water transport through the membrane.

Table 1. Comparison of recent TFN membranes to this work.

Nanofiller	Loading (wt%)	Water permeability ($L\ m^{-2}\ h^{-1}$ psi)	NaCl rejection	Reference
Bimodal silica	0.05% in hexane	0.178	95.7 ± 0.1%	This work
H-OMC	5% in water	0.158	48%	Kim et al. [18,19]
Zeolite	0.4% in hexane	0.0943	93.9 ± 0.3%	Jeong et al. [20]
MCM-41	0.05% in hexane	0.155	97.9 ± 0.3%	Yin et al. [26,27]
MWCNT	1.5% of polyamide in DMAc	0.052	32 ± 0.7%	Shawky et al. [12,30,31]
GO	0.015% in hexane	0.198	93.8 ± 0.6%	Yin et al. [35]

4. Conclusions

Novel BSNs/PA enhanced TFN membranes were prepared through an in situ IP process of

aqueous MPD and TMC-BSNs organic mixture solution. The BSN loadings were varied from 0 wt% to 0.1 wt%. The membrane performance and topography were significantly influenced by embedding BSNs, and the TFN membranes had an improved overall performance by loading certain amount of BSNs. With increasing BSNs concentration, the hydrophilicity and, the surface roughness of the membranes all increased. The water permeability increased from 38 ± 2.2 to 53.5 ± 5.5 L m^{-2} h^{-1}, nearly a 40% increase with near constant salt rejection. However, when the loading concentration of BSNs further increased beyond 0.05 wt% in the TMC-hexane organic solution, the aggregation of BSNs resulted in a worse dispersion of BSNs on the surface the TFN membrane, leading to a decrease in water permeability. Overall, BSNs NPs, with micro-mesoporous structure, is a good filler for being incorporated into the PA layer to enhance the performance of TFN membrane.

Acknowledgements

We greatly thank for N_2 adsorption/desorption analysis provided by Mr. Ali Tekeei in Professor Galen Suppes' group. We also thank Professor Qingsong Yu in the Department of Mechanical & Aerospace Engineering at MU for providing us the contact angle measurement characterization technique and AFM in Dr. Patrick Pinhero's lab.

Conflict of interest

All authors declare no conflicts of interest in this paper.

References

1. Mezher T, Fath H, Abbas Z, et al. (2011) Techno-economic assessment and environmental impacts of desalination technologies. *Desalination* 266: 263-273.
2. Su J, Zhang S, Ling MM, et al. (2012) Forward osmosis: an emerging technology for sustainable supply of clean water. *Clean Technol Envir* 14: 507-511.
3. Fritzmann C, Löwenberg J, Wintgens T, et al. (2007) State-of-the-art of reverse osmosis desalination. *Desalination* 216: 1-76.
4. Lee KP, Arnot TC, Mattia D (2011) A review of reverse osmosis membrane materials for desalination—Development to date and future potential. *J Membrane Sci* 370: 1-22.
5. Xu J, Wang Z, Yu L, et al. (2013) A novel reverse osmosis membrane with regenerable anti-biofouling and chlorine resistant properties. *J Membrane Sci* 435: 80-91.
6. Daraei P, Madaeni SS, Salehi E, et al. (2013) Novel thin film composite membrane fabricated by mixed matrix nanoclay/chitosan on PVDF microfiltration support: Preparation, characterization and performance in dye removal. *J Membrane Sci* 436: 97-108.
7. Zhu X, Loo HE, Bai R (2013) A novel membrane showing both hydrophilic and oleophobic surface properties and its non-fouling performances for potential water treatment applications. *J Membrane Sci* 436: 47-56.
8. Li D, Wang H (2010) Recent developments in reverse osmosis desalination membranes. *J Mater Chem* 20: 4551.

9. Wei J, Jian X, Wu C, et al. (2005) Influence of polymer structure on thermal stability of composite membranes. *J Membrane Sci* 256: 116-121.
10. Kim HI, Kim SS (2006) Plasma treatment of polypropylene and polysulfone supports for thin film composite reverse osmosis membrane. *J Membrane Sci* 286: 193-201.
11. Chen G, Li S, Zhang X, et al. (2008) Novel thin-film composite membranes with improved water flux from sulfonated cardo poly(arylene ether sulfone) bearing pendant amino groups. *J Membrane Sci* 310: 102-109.
12. Tarboush BJA, Rana D, Matsuura T, et al. (2008) Preparation of thin-film-composite polyamide membranes for desalination using novel hydrophilic surface modifying macromolecules. *J Membrane Sci* 325: 166-175.
13. Yu S, Liu M, Liu X, et al. (2009) Performance enhancement in interfacially synthesized thin-film composite polyamide-urethane reverse osmosis membrane for seawater desalination. *J Membrane Sci* 342: 313-320.
14. Mansourpanah Y, Momeni Habili E (2013) Preparation and modification of thin film PA membranes with improved antifouling property using acrylic acid and UV irradiation. *J Membrane Sci* 430: 158-166.
15. Zhao L, Chang PCY, Yen C, et al. (2013) High-flux and fouling-resistant membranes for brackish water desalination. *J Membrane Sci* 425-426: 1-10.
16. Li S, Wang Z, Zhang C, et al. (2013) Interfacially polymerized thin film composite membranes containing ethylene oxide groups for CO2 separation. *J Membrane Sci* 436: 121-131.
17. Buonomenna MG (2013) Nano-enhanced reverse osmosis membranes. *Desalination* 314: 73-88.
18. Johansson EM, Ballem MA, Cordoba JM, et al. (2011) Rapid synthesis of SBA-15 rods with variable lengths, widths, and tunable large pores. *Langmuir* 27: 4994-4999.
19. Kim E-S, Deng B (2011) Fabrication of polyamide thin-film nano-composite (PA-TFN) membrane with hydrophilized ordered mesoporous carbon (H-OMC) for water purifications. *J Membrane Sci* 375: 46-54.
20. Jeong BH, Hoek EMV, Yan Y, et al. (2007) Interfacial polymerization of thin film nanocomposites: A new concept for reverse osmosis membranes. *J Membrane Sci* 294: 1-7.
21. Jadav GL, Singh PS (2009) Synthesis of novel silica-polyamide nanocomposite membrane with enhanced properties. *J Membrane Sci* 328: 257-267.
22. Rajaeian B, Rahimpour A, Tade MO, et al. (2013) Fabrication and characterization of polyamide thin film nanocomposite (TFN) nanofiltration membrane impregnated with TiO2 nanoparticles. *Desalination* 313: 176-188.
23. Yin J, Zhu G, Deng B (2013) Multi-walled carbon nanotubes (MWNTs)/polysulfone (PSU) mixed matrix hollow fiber membranes for enhanced water treatment. *J Membrane Sci* 437: 237-248.
24. Dumée L, Lee J, Sears K, et al. (2013) Fabrication of thin film composite poly(amide)-carbon-nanotube supported membranes for enhanced performance in osmotically driven desalination systems. *J Membrane Sci* 427: 422-430.
25. Kim CE, Yoon JS, Hwang HJ (2008) Synthesis of nanoporous silica aerogel by ambient pressure drying. *J Sol-Gel Sci Techn* 49: 47-52.
26. Yin J, Kim ES, Yang J, et al. (2012) Fabrication of a novel thin-film nanocomposite (TFN)

membrane containing MCM-41 silica nanoparticles (NPs) for water purification. *J Membrane Sci* 423-424: 238-246.
27. Wu H, Tang B, Wu P (2013) Optimizing polyamide thin film composite membrane covalently bonded with modified mesoporous silica nanoparticles. *J Membrane Sci* 428: 341-348.
28. Mori H, Uota M, Fujikawa D, et al. (2006) Synthesis of micro-mesoporous bimodal silica nanoparticles using lyotropic mixed surfactant liquid-crystal templates. *Micropor Mesopor Mat* 91: 172-180.
29. Kosmulski M (2002) The pH-dependent surface charging and the points of zero charge. *J Colloid Interface Sci* 253: 77-87.
30. Lee HS, Im SJ, Kim JH, et al. (2008) Polyamide thin-film nanofiltration membranes containing TiO2 nanoparticles. *Desalination* 219: 48-56.
31. Shawky HA, Chae SR, Lin S, et al. (2011) Synthesis and characterization of a carbon nanotube/polymer nanocomposite membrane for water treatment. *Desalination* 272: 46-50.
32. Viart N, Niznansky D, Rehspringer JL (1997) Structural Evolution of a Formamide Modified Sol--Spectroscopic Study. *J Sol-Gel Sci Techn* 8: 183-187.
33. Wu H, Tang B, Wu P (2013) Optimization, characterization and nanofiltration properties test of MWNTs/polyester thin film nanocomposite membrane. *J Membrane Sci* 428: 425-433.
34. Yin J, Deng B (2015) Polymer-matrix nanocomposite membranes for water treatment. *J Membrane Sci* 479: 256-275.
35. Yin J, Zhu G, Deng D (2016) Graphene oxide (GO) enhanced polyamide (PA) thin-film nanocomposite (TFN) membrane for water purification. *Desalination* 379: 93-101.

AIMS Press

© 2016 Baolin Deng et al., licensee AIMS Press. This is an open access article distributed under the terms of the Creative Commons Attribution License (http://creativecommons.org/licenses/by/4.0)